Molecular dynamics simulations of the nano-droplet impact process on hydrophobic surfaces *

Hu Hai-Bao(胡海豹)†, Chen Li-Bin(陈立斌), Bao Lu-Yao(鲍路瑶), and Huang Su-He(黄苏和)

School of Marine Science and Technology, Northwestern Polytechnical University, Xi'an 710072, *China*

(Received 1 August 2013; revised manuscript received 22 November 2013; published online 8 May 2014)

Large-scale molecular dynamics simulations are used to study the dynamic processes of a nano-droplet impacting on hydrophobic surfaces at a microscopic level. Both the impact phenomena and the velocity distributions are recorded and analyzed. According to the simulation results, similar phenomena are obtained to those in macro-experiments. Impact velocity affects the spread process to a greater degree than at a level of contact angle when the velocity is relatively high. The velocity distribution along the X axis during spread is wave-like, either W- or M-shaped, and the velocity at each point is oscillatory; while the edges have the highest spread velocity and there are crests in the distribution curve which shift toward the edges over time. The distribution along the Y axis is <- or >-shaped, and the segments above the middle have the lowest decrease rate in the spreading process and the highest increase rate in the retraction process.

Keywords: nano-droplet, hydrophobic surface, molecular dynamics, velocity distribution

PACS: 47.55.dr, 47.61.–k, 47.11.–j **DOI:** 10.1088/1674-1056/23/7/074702

1. Introduction

Droplet impact on solid surfaces is a common phenomenon in nature, traffic, agriculture and industry. With the development of new energy resources and the fields of aviation and spaceflight, macro- or nano-scale droplet properties have attracted considerable attention because of their great investigative value and commercial potential. For example, the application of controlling droplet behavior in the proton exchange membrane fuel cell is a pivotal issue in dealing with the dewatering problem in the fuel cell.[1,2] In addition, due to its good properties of water-repellency and drag-reduction, hydrophobic surfaces have become a hot research subject.[3–5] The technology of their fabrication is rapidly developing, making it possible for hydrophobic surfaces to be widely used in many fields in the future. Therefore, research on droplets impacting on hydrophobic surfaces may be another way to understand the behaviors and inner mechanisms of droplets.

Experimental research on macro-droplet impacts on hydrophobic surfaces has been reported over the last decade. Chen and Li,[5] Hu *et al.*[6] have reported on rebound behavior. Li *et al.*[7] have studied the impact process and derived a function to calculate the contact time of liquid–solid interactions. The spread behavior obtained by using experimental methods was reported, and models were developed.[7–10] Though the macro-droplets have been extensively studied, the nature and mechanism of micro-droplet behavior still needs to be studied. Due to the obstacles in both generation and observation, it is difficult to study nano-droplets experimentally. For these reasons, simulation methods using molecular dynamics (MD) are employed to study micro-droplets and nano-droplets, since molecular dynamics can track all atomic trajectories, cover the collective behavior of a group of atoms and describe the details of interactions among the atoms. Most studies on droplets using MD are about the static and dynamic dewetting of droplets on solid surfaces with different wetting properties.[11–16] To study droplet behavior and inner dynamics well, research on dynamical motion and velocity distribution of nano-droplets is still needed.

In this paper, we focus on the dynamic processes of nano-droplet impacts on surfaces with different hydrophobicities by building up a nano-scale model through a molecular dynamics simulation. Droplet impact processes with different velocities on three kinds of surfaces are presented. The behaviors after impact are demonstrated and the influences of velocity and wetting properties on the spread of droplets after impact are compared under several different conditions. The velocity distributions along both the X and Y axes are analyzed to present the rules of velocity variation.

2. Model and method

In these molecular dynamics simulations, we consider a single droplet impact on hydrophobic surfaces under the condition of different velocities. The nano-droplet is formed at low temperature with 29449 argon atoms interacting with the Lennard–Jones (L–J) 12–6 pair potential,

$$\phi(r) = 4\varepsilon[(\sigma/r)^{12} - (\sigma/r)^{6}]. \quad (1)$$

Here, r represents the distance between two atoms, ε is the energy parameter, and σ is the length parameter. To model

*Project supported by the National Natural Science Foundation of China (Grant No. 51109178) and the Science and Technology Innovation Foundation of Northwestern Polytechnical University, China (Grant No. JC20120218).

†Corresponding author. E-mail: huhaibao@nwpu.edu.cn

© 2014 Chinese Physical Society and IOP Publishing Ltd

an Ar droplet, the parameter values in Eq. (1) are taken to be $\varepsilon = 1.67 \times 10^{-21}$ J and $\sigma = 3.405$ Å (Ar–Ar). The wall–wall (Pt–Pt) interaction parameters are $\varepsilon = 1.67 \times 10^{-21}$ J and $\sigma = 3.405$. For the vapor phase in the model, the density, atom mass and potential parameters refer to those of the real vapor. The cutoff radius is taken to be $r = 2.5\sigma_{(\mathrm{Ar-Ar})} = 8.5125$ Å for the L–J potential, and then is used for all interactions to reduce computational time. To indicate the difference in wetting properties between liquid and solid surfaces, another L–J pair potential between Ar and Pt is adopted as[15]

$$\phi_{\mathrm{ArS}} = 4\varepsilon_{\mathrm{ArPt}}\left[(\sigma_{\mathrm{ArPt}}/r)^{12} - (\sigma_{\mathrm{ArPt}}/r)^{6}\right]. \tag{2}$$

For interactions between Ar atom and Pt atoms, the parameters are chosen to be $\varepsilon_{\mathrm{ArPt}} = 0.894 \times 10^{-21}$ J and $\sigma_{\mathrm{ArPt}} = 3.085$ Å. The molar mass values used in the simulation are 39.948 g/mol for Ar and 195.09 g/mol for Pt.

The contact angle is calculated according to the following function:[15]

$$\cos\theta = 2\varepsilon_{\mathrm{ArPt}}/\varepsilon - 1. \tag{3}$$

Surfaces with different wetting properties are achieved by adjusting $\varepsilon_{\mathrm{ArPt}}$, which is the energy parameter between Ar and Pt atoms. The corresponding values between contact angle (CA) and $\varepsilon_{\mathrm{ArPt}}$ are listed in Table 1.

Table 1. Corresponding values between CA and ε.

CA/(°)	110	130	150
$\varepsilon_{\mathrm{ArPt}}$/J	0.003428	0.001861	0.000698

A three-dimensional (3D) droplet impact model is built up, which includes a droplet and two smooth solid surfaces as shown in Fig. 1. The entire model has the dimensions 288 Å×288 Å×291 Å (length×width×height). Periodic boundary conditions are all imposed in the x, y and z directions. The upper wall is just used to prevent liquid atoms from crossing the upper boundary. Therefore it is constructed into a single layer. The lower wall is constructed into the fcc lattice structure with a lattice constant 3.9242 Å using 143035 Pt atoms. The embedded atom method (EAM) potential is utilized to describe the lower wall, and to simulate the impact process properly, three types of Pt atoms are adopted in the lower wall, namely fixed atoms, thermostat atoms and Newtonian atoms.[17] These atoms are fixed on their lattice sites to prevent the lower wall from moving, which comprises the bottom two layers of atoms. The middle four layers of atoms, defined as the thermostat atoms, are used to control the temperature. The Newtonian atoms comprise the top seven layers of substrate atoms. The motions of thermostat atoms and Newtonian atoms are determined by Newton's equations of motion. The thickness of Newtonian atoms is set to be 11.7726 Å ($> r_c$) to eliminate the effect of it. In the simulation, an NVE ensemble is used to update the velocities and positions of liquid atoms and Newtonian atoms at each time step, and an NVT ensemble is used for thermostat atoms. The Verlet algorithm is adopted to calculate the motion of the particles in time steps of 0.002 ps.

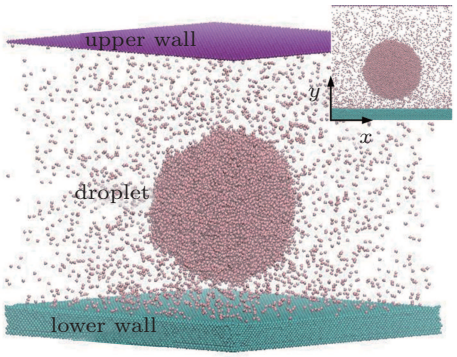


Fig. 1. (color online) The 3D droplet-impact model based on MD. The inset shows the front view of the model.

At the beginning of the simulation, the argon droplet is placed far from the surface and the simulation box is also filled up with vapor atoms. Before impact, the velocities and positions of the liquid atoms are refreshed at each time step and the temperature is held at 85 K by renormalizing the speeds of the constituent atoms to keep their kinetic energy constant. Furthermore the temperature of the surface is maintained at 85 K using the Nosé–Hoover thermostat. For the real thermal exchange to take place, the thermal control of the liquid is cancelled when the droplet falls off and impacts on the surface. The atom number and the velocity of each slice are recorded every 2000 time steps (4 ps).

3. Results and discussion

3.1. Impact phenomenon

In macro-scale experiments, the behaviors of many droplets after impact, such as attachment, rebound and splash, have been observed by several researchers.[3–9] In the simulation results, different droplet behaviors are also obtained under different velocities or on surfaces with different wetting properties. The spread, attachment, rebound and splash behaviors shown in Fig. 2 are in concordance with the common behaviors of droplets in macro-scale experiments.

While the behaviors are similar in micro- and macro-experiments, the experimental conditions are quite different. As indicated in our earlier study,[6] the critical velocities for millimeter-scale droplets to deform on hydrophobic surface are lower than 2 m/s, while in the simulations, the nano-droplet can hardly deform even when velocity is 10 m/s (Fig. 2(a)). There are two simple explanations we analyze to explain this difference.

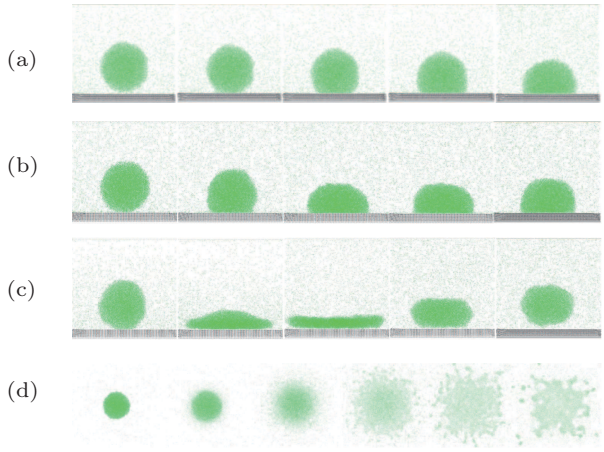


Fig. 2. (color online) Typical behaviors of droplet impact on a surface at different velocities. Panel (a) shows barely deformation ($v = 10$ m/s, $\theta = 110°$), panel (b) the attachment ($v = 50$ m/s, $\theta = 110°$), panel (c) the rebound case ($v = 200$ m/s, $\theta = 150°$), and panel (d) the splash ($v = 400$ m/s, $\theta = 110°$).

In the spread process, the kinetic energy of droplets is converted into energy dissipation and surface energy. The energy of dissipation is mainly due to viscous dissipation and the work (W_1) done against viscosity, which is approximately given as[6]

$$W_1 \approx \frac{\pi\rho D_0 D_{\max}^2 V_0^2}{3\sqrt{Re}}, \tag{4}$$

where D_0 and $D_{\max}$ are the initial diameter and the maximum diameter of the nano-droplet in the spread process, and Re is the Reynolds number of the nano-droplet. The equations to calculate initial kinetic energy (E_v) and surface energy (E_s) during spreading are

$$\begin{aligned} E_v &= \pi\rho D^3 v^2/12, \\ E_s &= 0.24\pi D_{\max}^2 \sigma(1-\cos\theta). \end{aligned} \tag{5}$$

When the droplet spreads and reaches its maximum diameter, it satisfies

$$E_v - E_s - W_1 = 0. \tag{6}$$

Substitution of Eqs. (4) and (5) into Eq. (6) yields

$$\frac{1}{k} = \frac{D_0^2}{D_{\max}^2} = \frac{\sqrt{\rho D_0 V \mu}V/3 + 0.24\sigma(1-\cos\theta)}{\rho D_0 V^2/12}. \tag{7}$$

In this equation, we define k as a parameter to measure the level of deformation. According to Eq. (7), it can be concluded that k increases as V increases while it decreases as D_0 decreases. In other words, for droplets with the same dimensions, the higher the velocity, the easier the droplet deforms. However for the droplets with the same velocity, the smaller the droplet, the more difficult it is to deform. In another explanation based on fluid mechanics, surface tension results in the differential pressure on two sides of a curved surface, which is calculated as follows:

$$P_d = \sigma(1/R_1 + 1/R_2), \tag{8}$$

where R is the radius and P_d is the differential pressure. For a droplet, R_1 and R_2 are equal, so that equation (8) reduces to $P_d = 2\sigma/R$. In this equation, the smaller the droplet, the larger the pressure will be. Therefore, it is more difficult to deform a droplet with a tiny radius.

Both of these reasons explain why small droplets begin to deform at quite high velocities. With a combination of the simulation results and these explanations, MD is believed to be an efficient way to study the dynamics of droplet impacts.

3.2. Influences on spread behavior

Spread phenomenon is a typical behavior of droplet impact on surfaces and can help explain certain surface properties of interest, such as drag reduction. For a certain droplet, better drag reduction of surface leads to a larger spread diameter. In addition, other factors will influence the spread diameter, such as the surface roughness, wetting properties, the droplet diameter or the droplet velocity. In this simulation, we focus on the influences of droplet impact velocity and the surface wetting property.

To examine the extent of impact velocity and surface contact angle effects, droplet impact experiments are simulated on three surfaces (shown in Table 1) and with four impact velocities for each surface. The prime diameter (D_0) is taken to be 137.032 Å (1 Å = 10^{-10} m). The simulation results of each surface are recorded and treated. To present the influence of impact velocity on the spread behavior, the variations of diameter on surfaces with $\theta = 110°$ and $\theta = 130°$ under different velocities are shown in Fig. 3.

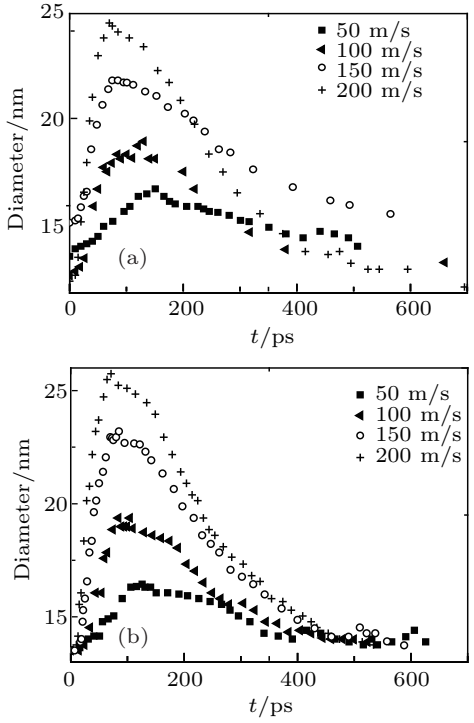


Fig. 3. The laws of spread diameter against time on different surfaces at four velocities at $\theta = 110°$ (a) and 130° (b).

Although there are some differences among the spread behaviors on different surfaces, the general spread rules appear to be similar. As shown in Fig. 3, the spread diameter is a function of impact velocity. A higher impact velocity leads to a shorter spread time and a longer retraction time, which makes the total time (contact time) from impact to an almost steady state unchanged. On the same surface, the contact time is similar to that on different surfaces. In addition, a higher velocity results in a larger spread diameter, which could be twice as large as D_0. In the retraction process, the spread diameter will oscillate several times before it finally becomes steady as shown in Fig. 3. This effect can also be seen in dynamic process photographs of the simulation.

In addition to impact velocity, the surface wetting property (usually represented by CA) is another factor that influences spread behavior, which is confirmed in macro-experiments. Figure 4 demonstrates the spread laws of droplet impacts on different surfaces with the same velocities. Each panel presents the spreading behavior on three surfaces with the same velocities. According to the results, we find that there is little distinction among different surfaces. In other words, the surface wetting property has little effect on the spreading process even at a relatively high velocity. From Figs. 3 and 4, it can be concluded that at a relatively high velocity, the impact velocity affects the spreading process more strongly than the surface property.

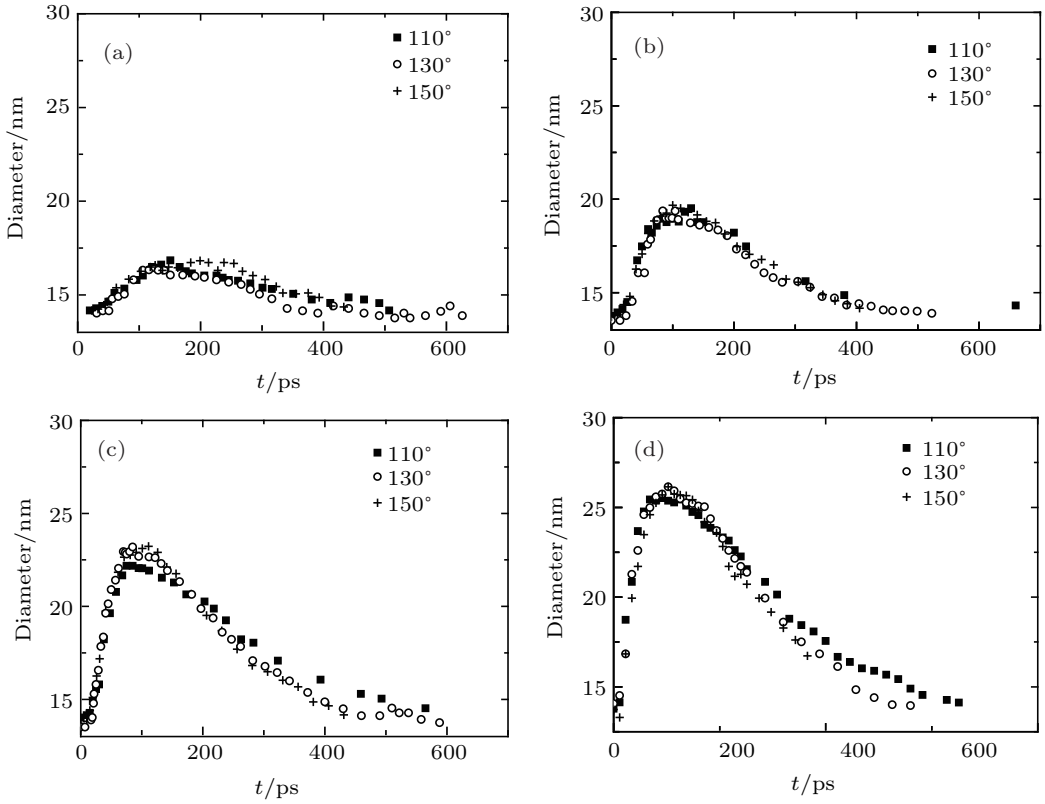


Fig. 4. Droplet spread laws on different hydrophobic surfaces at four velocities: (a) 50 m/s, (b) 100 m/s, (c) 150 m/s, and (d) 200 m/s.

3.3. Velocity distribution

The velocity distribution is another important factor in the droplet impact study, though it is seldom reported. In previous researches, at the impact moment or in the impact process, the velocity variation was unknown or approximated as a stagnation-flow speed. In this aspect, to study the velocity variation along the X axis and Y axis in the spread process, the droplet impact model is divided into 2000 segments along the X axis and 2000 segments along the Y axis, and the average velocity of each of those segments is recorded every 2000 time steps (4 ps). Several typical moments are chosen as shown in Figs. 5 and 6. As similar laws are found for different surfaces at different velocities, the resulting 1D velocity distribution (110°, 100 m/s) is presented as follows.

At the beginning the initial velocity direction is in the negative Y direction, and at the very beginning, the horizontal velocities of all segments are not distributed homogeneously (Fig. 5(a)). Then the vertical kinetic energy is converted into horizontal kinetic energy and surface energy when the droplet spreads, and thus causes the horizontal velocity to increase (Figs. 5(b) and 5(c)). When all vertical energies have been converted into the droplet surface energy and horizontal kinetic energy, the droplet's horizontal kinetic energy continues to convert into surface energy until the kinetic energy decreases to

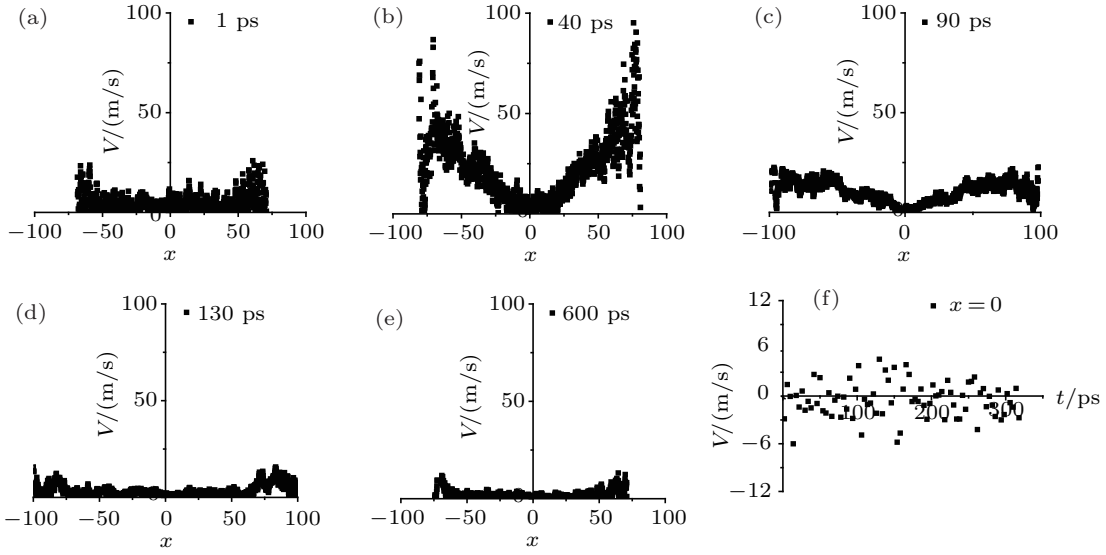


Fig. 5. Horizontal velocity distribution along the X axis at several moments: (a) $t = 1$ ps, (b) $t = 40$ ps, (c) $t = 90$ ps, (d) $t = 130$ ps, (e) $t = 600$ ps, and (f) $x = 0$.

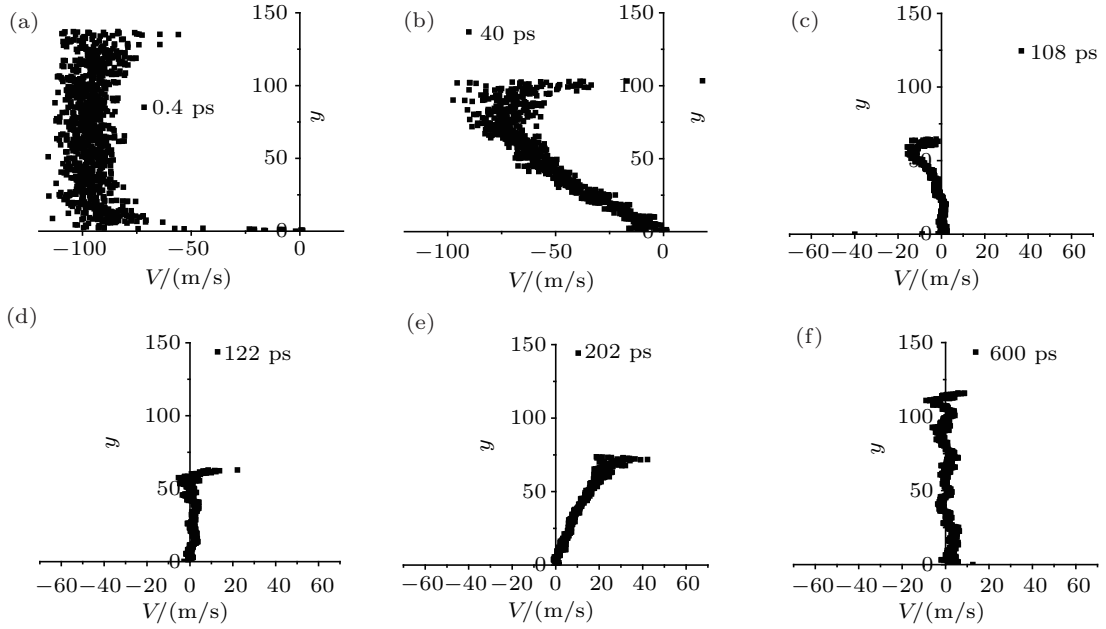


Fig. 6. Velocity distributions along the Y axis at different times: (a) $t = 0.4$ ps, (b) $t = 40$ ps, (c) $t = 108$ ps, (d) $t = 122$ ps, (e) $t = 202$ ps, and (f) $t = 600$ ps.

zero, at which moment the velocities of all segments are almost uniformly distributed (Fig. 5(e)). As shown in Figs. 5(a)–5(c), the shape of the velocity distribution along the X axis during the spread is wave-like, either W- or M-shaped. The M shape appears mostly in the spread process, but the velocity of the central segment does not remain at zero or is not unchanged (Fig. 5(f))—it oscillates with time. The absolute value of the velocity of the center increases until the spread diameter reaches its maximum and then decreases as the droplet retracts as shown in Fig. 5(d). Not only does the velocity of a partial segment oscillates with time, but the velocities of all the segments at a given moment will oscillate along the distance (Figs. 5(a)–5(e)). In the distribution curve, there are two crests appearing in the area between the edge and the center which have the highest velocity and ascending rate (Fig. 5(b)). As time goes by, the crests shift toward the edge. When the spread process tends to be steady, the velocity of each segment decreases and the velocities of all the segments are nearly the same (Fig. 5(e)).

The velocity distribution along the Y axis is totally different as shown in Fig. 6. At the beginning, the vertical velocities of all segments are negative, and the velocities of the segments near the surface become zero after impact, while the remaining segments remain unchanged. Then, the velocity decreases from a certain height to the bottom, and also decreases as the distance grows to the top, which presents a $<$ shape, while

velocities of several segments of the bottom become positive. As the results show, the vertical velocity of the whole droplet does not become zero at the time when the droplet reaches its maximum spread diameter, but it is almost zero at an earlier moment (Fig. 6(d)). When the droplet deforms most, all the velocities have already become positive (132 ps). After that, the velocity begins to increase towards the positive and then decreases to zero, displaying a $>$ shape. The velocities of all the segments vanish when the droplet finally becomes steady.

In the whole impact process, the distribution curve waves while the crest does not appear at the top nor at the bottom but it appears in the area around the middle in both the X axis and the Y axis. In the distribution along the X axis, the distribution curve is W- or M-shaped. While in the Y axis, the curve is $<$- or $>$-shaped and the area above the middle has the lowest descending rate and highest ascending rate.

4. Conclusions

In this paper, a simulation is conducted using molecular dynamics to study the process of a nano-droplet's impact on hydrophobic surfaces. Similar phenomena are recorded in simulations as in these experiments. On the basis of the simulation results, this method can be used to not only simulate the dynamic process of nano-droplet impact on hydrophobic surfaces with different wetting properties, but also to describe the interior velocity distribution in the impacting droplet, which is more detailed than those observed in macroscopic experiments. Therefore, this method is thought to be an efficient way to study and analyze the behavior and dynamical mechanisms of impacting droplets.

References

[1] Praven K C and Finnerty C M 2006 *J. Power Sources* **160** 490
[2] Jiao K and Li X G 2011 *Prog. Energy Combust. Sci.* **37** 221
[3] Merlen A and Brunet P 2009 *J. Bionic Eng.* **6** 330
[4] Brown P S, Berson A and Talbot E L 2011 *Langmuir* **27** 13897
[5] Chen L Q and Li Z G 2010 *Phys. Rev. E* **82** 016308
[6] Hu H B, Chen L B, Huang S H and Song B W 2013 *Sci. China Phys. Mech.* **56** 960
[7] Li X Y, Ma X H and Zhong L 2010 *Langmuir* **26** 4831
[8] Gu Y G and Li D Q 2000 *Colloid. Surf. A* **163** 239
[9] Anderson D M, Forest M G and Superfine R 2001 *Sian. J. Appl. Math.* **61** 1502
[10] Sun Z H and Han R J 2008 *Chin. Phys. B* **17** 3185
[11] Bertrand E, Blake T D, Ledauphin V, Ogonowski G and Coninck J D 2007 *Langmuir* **23** 3774
[12] David R H, Gary S G, Edmund B W III 2005 *Phys. Rev. Lett.* **95** 107801
[13] Blake T D and Coninck J D 2002 *Adv. Colloid. Interface.* **96** 21
[14] Yan Y Y and Ji C Y 2008 *J. Bionic Eng.* **5** 271
[15] Cao B Y, Chen M and Guo Z Y 2006 *Acta. Phys. Sin.* **55** 5305 (in Chinese)
[16] Coninck J D and Blake T D 2008 *Annu. Rev. Mater. Res.* **38** 1
[17] Zhang J, Liu C, Shu Y H and Fan J 2012 *Appl. Surf. Sci.* **261** 690